Direct-synthesis method towards copper-containing periodic mesoporous organosilicas : detailed investigation of the copper distribution in the material

Reference:

Lin Feng, Meng, Kukueva Elena, Altantzis Thomas, Mertens Myrjam, Bals Sara, Cool Pegie, Van Doorslaer Sabine.- Direct-synthesis method towards copper-containing periodic mesoporous organosilicas : detailed investigation of the copper distribution in the material

Journal of the Chemical Society: Dalton transactions / Chemical Society [London] - ISSN 1477-9226 - 44:21(2015), p. 9970-9979

DOI: http://dx.doi.org/doi:10.1039/c4dt03719g

Handle: http://hdl.handle.net/10067/1264220151162165141

Direct-synthesis method towards copper-containing periodic mesoporous organosilicas: detailed investigation of the copper distribution in the material

Feng Lin,[a,b] Xiangyan Meng,[a] Elena Kukueva,[c] Thomas Altantzis,[c] Myrjam Mertens,[d] Sara Bals,[c] Pegie Cool[a]* and Sabine Van Doorslaer[b]*

[a] Laboratory of Adsorption and Catalysis, Department of Chemistry, University of Antwerp, Universiteitsplein 1, B-2610, Wilrijk, Belgium.

E-mail: pegie.cool@uantwerpen.be; Fax: +32 3 2652374;

Tel: +32 3 2652355

[b] BIMEF Laboratory, Department of Physics, University of Antwerp, Universiteitsplein 1, B-2610, Wilrijk, Belgium.

E-mail: sabine.vandoorslaer@uantwerpen.be; Fax: +32 3 2652470;

Tel: +32 3 2652461

[c] EMAT, Department of Physics, University of Antwerp, Groenenborgerlaan 171, B-2020, Antwerpen, Belgium.

[d] Flemish Institute for Technological Research, VITO, Boerentang 200, B-2400, Mol, Belgium

Abstract

Three-dimensional cubic Fm3m mesoporous copper-containing ethane-bridged PMO materials have been prepared through a direct-synthesis method at room temperature in the presence of cetyltrimethylammonium bromide as surfactant. The obtained materials have been unambiguously characterized in detail by several sophisticated techniques, including XRD, UV-Vis-Dr, TEM, elemental mapping, continuous-wave and pulsed EPR spectroscopy. The results show that at lower copper loading, the Cu^{2+} species are well dispersed in the Cu-PMO materials, and mainly exist as mononuclear Cu^{2+} species. At higher copper loading amount, Cu^{2+} clusters are observed in the materials, but the distribution of the Cu^{2+} species is

still much better in the Cu-PMO materials prepared through the direct-synthesis method than in a Cu containing PMO material prepared through an impregnation method. Moreover, the evolution of the copper incorporation during the PMO synthesis has been followed by EPR. The results show that the immobilization of the Cu^{2+} ion/complex and the formation of the PMO materials are taking place simultaneously. The copper ions are found to be situated on the inner surface of the mesopores of the materials and are accessible, which will be beneficial for the catalytic applications.

Introduction

The synthesis of mesoporous materials with uniform pore size and high specific surface areas has opened unique possibilities in the field of adsorption and catalysis. Over the past decade, significant progress has been made in the preparation of various mesoporous materials. Among the most recent innovations, the synthesis of periodic mesoporous organosilicas (PMOs), which contain organic groups as an integral part of the inorganic-oxide framework, marks an important progress in this field of research.[1,2] In contrast to the organically functionalized mesoporous silicas, PMOs have inorganic and organic moieties that are covalently linked to each other and homogeneously distributed in the framewall. With this, the research of mesoporous materials has moved from a "chemistry of the void space" to a "chemistry of the walls".[3] Moreover, the organic groups in the framewall can be chemically modified. PMOs with a variety of organic groups have been synthesized,[4] leading to promising materials for catalysis, metal scavenging and controlled drug release.

Similar to pure silica-based mesoporous materials, the lack of active sites in PMOs limits their use in catalysis. It is well known that the introduction of transition-metal ions into a silicate framework is one of the most efficient ways to create active catalytic sites. In addition, due to the highly hydrophobic surface properties of PMO materials, it is generally expected that PMO materials functionalized with metal species may offer significant advantages over the traditional pure silica-based materials.[5,6] For instance, Alincorporation in PMOs leads to a higher hydrothermal stability and improved catalytic performance in alkylation reactions in comparison to Al-MCM-41 materials.[7] Ti-PMOs show high hydrophobicity and have been found to be effective catalysts for the epoxidation of alkenes[8] and ammoxidation of ketones to oximes[9]. So far, metal-containing PMO materials have been obtained by means of impregnation, grafting or direct-synthesis methods. Among these,

direct-synthesis procedures can offer much more advantages, since they usually lead to more stable and well-dispersed metal species in the material.[10] Nevertheless, several difficulties need to be overcome for the direct synthesis, such as the leaching of the metal species upon template removal and the loss of the ordered structure with respect to the metal loading. Until now, only a very limited number of transition-metal ions has been introduced into PMO materials via direct synthesis, i.e. Al[7,11-13], Ti[9,14-16], V[17], Cr[18].

Copper is of particular interest due to its special redox properties, low cost and its higher reduction potential with respect to other transition metals.[19] Copper-containing mesoporous materials have long been used as catalysts for a wide range of reactions,[20-24] whereby the copper sites in the framework and/or the highly dispersed copper species are considered as the active centers. Although copper-containing mesoporous materials have received considerable attention, the reports on copper-containing PMO materials are very scarce. The first attempt in this sense was reported by Corriu and co-workers who inserted Cu-cyclam complexes in the silica framework.[25] More recently, copper ions were immobilized on bisimidazolium (BIM) ionic liquid-bridged PMO materials, and the obtained Cu-BIM-PMO shows high activity and stability in the decomposition of cyclohexyl hydroperoxide.[26] However, all of these Cu-containing PMO materials are obtained through a complicated post-synthesis process.

In the present work, a facile direct synthesis method of coppercontaining ethane-bridged PMO materials is described. The structure and sorption properties of the obtained materials were studied by Xray diffraction (XRD) and N2 adsorption-desorption, while the nature and distribution of the Cu^{2+} species was investigated using UV-visible diffuse reflectance (UV-Vis-Dr) spectroscopy, electron paramagnetic resonance (EPR) and transmission electron microscopy (TEM).

Experimental

Materials

All starting materials were used as purchased without further purification: 1,2-bis(triethoxysilyl)ethane (BTEE, 96%, Sigma- Aldrich), cetyltrimethylammonium bromide (CTABr, 99%, Sigma- Aldrich), ammonia solution (28%-30%, Acros Organic), copper(II) nitrate (Cu(NO3)2·3H2O, 99%, Acros Organic), ethanol (99.9%, Merck KGaA).

Synthesis of Cu-containing PMO materials

Precipitation of copper hydroxides was avoided by using an ammonia solution for the synthesis, since NH3 readily ligates Cu^{2+} cations. In a typical procedure, 0.48 g cetyltrimethylammonium bromide (CTABr) was dissolved in 14.9 g water, followed by addition of 8.5 ml of ammonia solution (28%-30%). Subsequently, a dark blue solution composed of an appropriate amount of Cu(NO3)2·3H2O and 3 ml ammonia solution was added into the above mixture. Finally, after stirring for about 30 mins, 2ml 1,2-bis(triethoxysilyl)ethane (BTEE) was drop-wise added. The final molar composition of the synthesis mixture is BTEE/CATBr/NH4OH/H2O/Cu(NO3)2·3H2O = 1:0.25:34.3:238:x, with x taken 0, 0.06, 0.1, 0.15, 0.2 or 0.3. The resulting mixture was continuously stirred at ambient temperature for 24 h. Then, the blue product was collected by filtration, washed thoroughly with water and dried at ambient conditions. Surfactant template removal was accomplished by three template extraction cycles with ethanol at 60°C to produce the mesopores. The obtained materials were subsequently calcined at 200°C for 16 h. The color of the calcined sample was turquoise (low copper content) to dark green (higher copper content). The samples are named xCu-PMO with x defined above.

In a second preparation method, Cu(NO3)2 was introduced into ethane-bridged PMOs by impregnation. In a standard procedure, 0.033g of Cu(NO3)2 was dissolved in 9 ml of deionized water, and 0.5 g of dried ethane-bridged PMOs was added. The suspension was stirred for 10 h at room temperature, and then, the water component was evaporated by mild heating (80°C) of the sample overnight. The sample is hereafter called IM-Cu-PMO.

Methods

N_2 adsorption–desorption isotherms were obtained at liquid N_2 temperature (77 K) using a Quantachrome Quadrasorb-SI automated gas adsorption system. Prior to adsorption, the samples were outgassed under high vacuum for 16 hours at 100 °C. The specific surface area was calculated using the Brunauer-Emmet-Teller method, for a relative pressure of 0.05 to 0.35. The pore-size distributions were deduced from the desorption branches of the isotherms using the Barrett-Joyner-Halenda method. The total pore volumes were calculated from the amount of N_2 vapor adsorbed at a relative pressure of 0.95.

XRD measurements were recorded on a Pananalytical X'PERT PRO MPD diffractometer with filtered CuKα-radiation. The measurements were performed in the 2θ mode using a bracket sample holder with a scanning speed of 0.04°/4 s continuous mode.

UV-Vis-Dr spectra were obtained at room temperature on a Nicolet Evolution 500 UV-Vis spectrometer, with a diffuse reflectance accessory (Thermo-electron RSA-UC40 integrating sphere) using BaSO4 standard as a reference. Samples were diluted with KBr to 2 wt%. The data were transferred according to equation:

$K = (1-R)^2/2R$

where K is reflectance transformed according to Kubelka-Munk, R is reflectancy (%).

The copper loading was determined by elemental analysis carried out on a JEOL JCXA 733 super-probe (electron probe microanalysis).

For the TEM measurements, the samples were dispersed in ethanol, crushed in an agate mortar and deposited on a carbon-coated molybdenum grid for energy dispersive X-ray (EDX) measurements and on a copper grid for TEM and high angle annular dark field scanning transmission electron microscopy (HAADF-STEM) measurements. TEM images and selected area electron diffraction (SAED) patterns were acquired using a FEI Tecnai G2 electron microscope operated at 200 kV. EDX maps and electron tomography series were acquired using an aberration-corrected cubed FEI Titan 60-300 electron microscope operated at 200 kV. For the acquisition of the EDX maps, a ChemiSTEM system was used and for the acquisition and quantification of the maps,[27] the ESPRIT software was used. For the electron tomography series, HAADF-STEM images were acquired in an angular range from -64° to +64° and a tilt increment of 2°, by using a Fischione model 2020 single tilt tomography holder. The alignment of the series was performed by a combination of an automated and manual alignment by using the FEI Inspect3D software and IMOD, respectively. The reconstruction was performed by using the Simultaneous Iterative Reconstruction Technique as implemented in the ASTRA toolbox using 150 iterations.[28] The reconstructed volume was visualized using the Amira 3D software.

X-band continuous wave (CW) EPR measurements were performed on a Bruker ESP 300E instrument, equipped with a liquid helium cryostat (Oxford Inc.), and working at a microwave (mw) frequency of about 9.5 GHz. An mw power of 1 mW, modulation frequency of 100 kHz and modulation amplitude of 0.05 mT were applied.

X-band pulsed EPR spectra were detected on a Bruker Elexsys E580 spectrometer operating at an mw frequency of 9.76 GHz. The spectrometer is equipped with a helium gas-flow cryostat (Oxford, Inc.).

Electron-spin-echo (ESE)-detected EPR experiments were carried out using the pulse sequence $\pi/2-\tau-\pi-\tau-$echo with $t\pi/2$ = 16 ns, $t\pi$= 32 ns, and the inter-pulse distance τ being varied from 96 ns to 2136 ns in steps of 8 ns.

The HYSCORE (hyperfine sublevel correlation spectroscopy) experiments[29] were performed using the $\pi/2$-τ-$\pi/2$-t1-π- t2-$\pi/2$-τ- echo sequence with pulse lengths $t\pi/2$= 16 ns, $t\pi$= 32 ns. The times t1 and t2 were varied from 96 to 4880 ns in steps of 16 ns. Experiments are performed for different τ values as specified in the figure caption.

Simulations of all EPR and HYSCORE spectra were performed with the EasySpin program, a MATLAB toolbox developed for EPR simulations.[30] The HYSCORE data were processed with MATLAB 7.7.0 (The MathWorks, Inc., Natick, MA). The time traces were baseline-corrected with a third-order polynomial, apodized with a Hamming window and zero-filled. After a two-dimensional Fourier transformation, the absolute spectra were computed. Spectra recorded with different τ values were added after Fourier transformation to eliminate blind-spot effects.

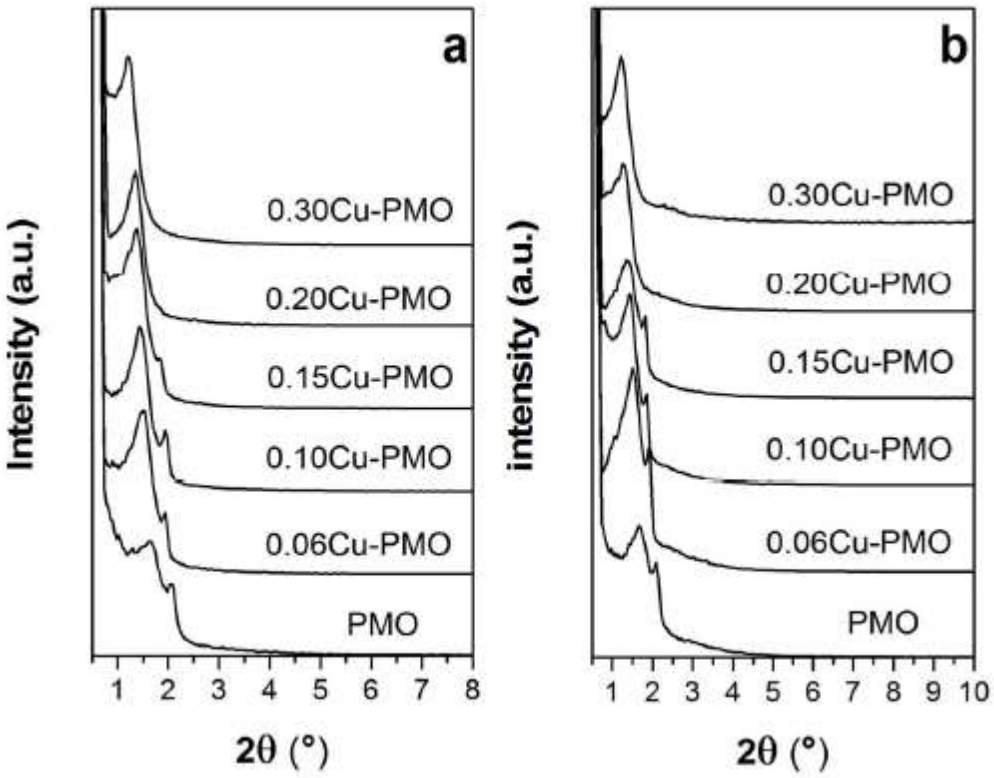

Figure 1. XRD patterns of the as-synthesized (a) and template-free (b) xCu-PMO samples with different amounts of copper (xCu-PMO: x refers to the molar ratio of Cu/BTEE in the synthesis mixture)

Results and discussion

The powder XRD patterns of the as-synthesized and template-free samples are shown in Figure 1. The XRD patterns of all samples exhibit a sharp diffraction peak and a small shoulder peak in the 2θ region from 1° to 3°. These peaks can be assigned to the (111) and (200) diffractions, respectively, of a face-centered-cubic Fm3 m mesoporous structure. The relative intensity of the (111) diffraction peak is much higher for the Cu-containing PMOs than for the PMOs without copper, indicating a better ordered mesostructure in the former PMOs. It suggests that the copper loading does not destroy the mesostructure, unlike what happens in the comparable synthesis of copper-containing MCM-41.[31] The TEM studies of the copperfree PMO materials are depicted in Figure S1 (Supporting Information). In Figure S1a, where a HAADF-STEM image is given, it can be clearly seen that the solvent-extracted copper-free sample shows hollow spherical morphology (bright spheres on dark background), which is typical for mesoporous silica materials synthesized with the assistance of ammonia.[32.33] Some hollow spheres are broken by the scraper during the TEM sample preparation process. Figure S1b shows a TEM image of the highly ordered mesoporous networks with a linear array of mesopores and walls, which is characteristic for a cubic Fm3m mesostructure. The image was acquired with under-focused conditions (the pores are represented white and the walls dark), in order to enhance the contrast from the pores. The same mesostructure is found for the Cucontaining PMOs materials (see TEM images in Figs. 2 and S2). However, besides the typical cubic Fm3m mesostructure signature, some distortion of the structure can be observed in the Cu-containing PMOs materials, especially in the samples with higher copper loading amount (Figure 2).

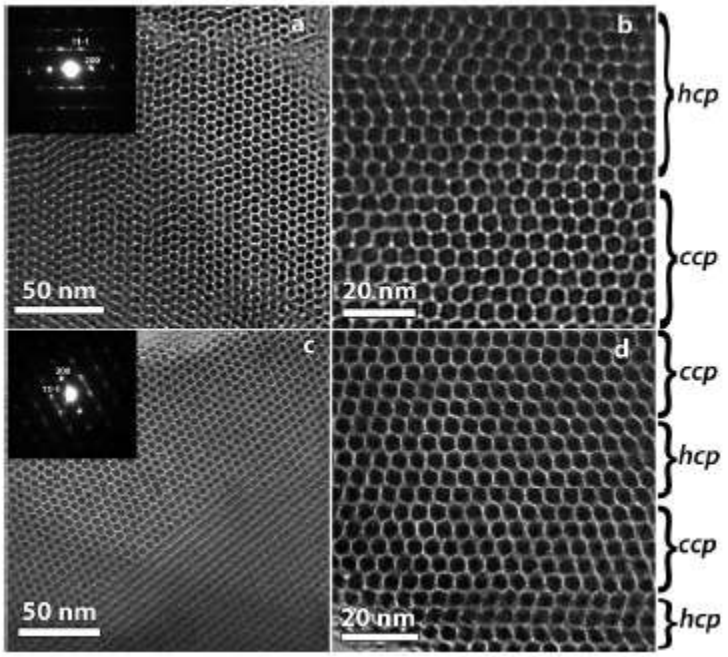

Figure 2. HRTEM images and electron diffraction patterns (insets) of solvent-extracted (a),(b) 0.06Cu-PMO, (c),(d) 0.30Cu-PMO. Images are acquired along [110] cubic axis

Note that, for the images of Figs. 2 and S2, over-focused conditions were used in order to enhance the pore contrast and to obtain a clearer visualization of the distortions. The pores are now represented dark and the walls white. An intergrowth of cpp (cubic close-packed) and hcp (hexagonal close-packed) structures is observed in the Cu-containing PMOs, which can also be evidenced by the streaks perpendicular to the layer in the SAED patterns as shown in the insets of Figure 2. These results indicate that the addition of copper species during the synthesis has led to some changes in the mesostructure of the PMO materials, which is in line with the gradual change of the shape of the XRD patterns with increasing of the copper content (Figure 1). Most likely, the copper species in the synthesis mixture act as auxiliary agents to enhance the self-assembly interaction. Moreover, since the $[Cu(NH3)4]^{2+}$ species are hydrophilic, part of them can penetrate into the surfactant micelles, and stay in the outer boundary, leading to an enlargement of the effective head-group area (a0). Hence, the surfactant packing parameter gP=V/a0l [34] will decrease with increasing copper amount in the synthesis mixture. Moreover, it is worth noting that the sharp diffraction peak of the Cu-containing PMOs gradually shifts to lower 2θ angles with increase of the copper content, which may indicate a possible insertion of divalent copper ions in the silicate framework of the PMO materials or an enlargement of the pore size.

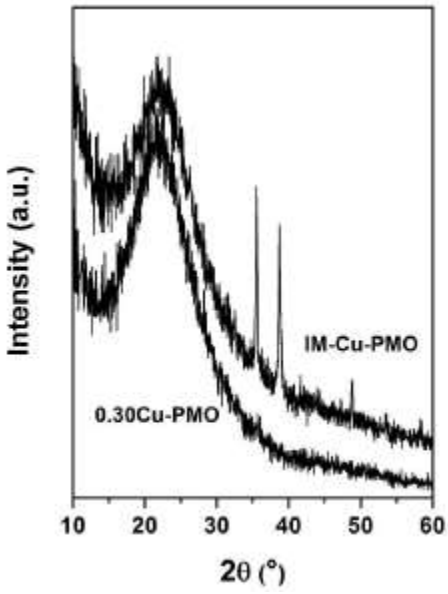

Figure 3. Wide-angle XRD pattern of 0.30Cu-PMO and IM-Cu-PMO

Figure 3 depicts the wide-angle XRD pattern of 0.30Cu-PMO in comparison to the one of a copper-containing PMO material prepared by impregnation (IM-Cu-PMO, 2 wt%). Both of them exhibit a broad peak at a 2θ-value of about 20°, which can be ascribed to the presence of amorphous SiO2.[35] For IM-Cu-PMO, two distinct diffraction peaks can be observed in the range of $30° < 2\theta < 40°$, typical of copper-oxide species. Such peaks are not observed in the wide-angle XRD pattern of 0.30Cu-PMO, suggesting that no crystalline copper oxide exists in this material[36], although amorphous copper-oxides may still be present (see also EPR and UVVis-DR analysis).

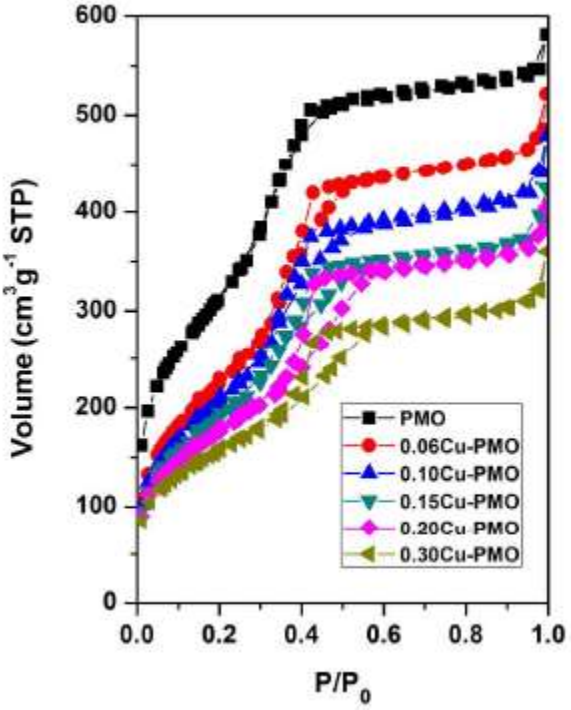

Figure 4. N_2 adsorption-desorption isotherms of the xCu-PMOs under study

All the nitrogen adsorption-desorption isotherms of the PMO materials presented in Figure 4 are of type IV (IUPAC), typical for mesoporous materials. A well-defined step occurs between P/P0= 0.2-0.5, which is due to the capillary condensation of N2 molecules in the mesopores. The corresponding pore-size distribution curves are shown in Figure S3, and the structural parameters are collected in Table 1. It can be seen from Table 1 that in comparison with the copper-free PMO materials, the pore diameter of all coppercontaining PMOs becomes larger. Furthermore, the specific surface area and pore volume of the copper-containing PMO materials gradually decrease with increasing copper loading. As a consequence, the specific surface area decreases from about 1014 m2g-1 for PMO without copper to about 845 m2g-1 for 0.06Cu-PMO (with 0.9% of copper) and to 572 m2g-1 for 0.30Cu-PMO (4.8% of copper) (Table 1). In addition, the hysteresis loop of the isotherms of the Cu-PMOs becomes larger with increasing copper content. The isotherms of 0.20Cu-PMO and 0.30Cu-PMO contain a typical H2 hysteresis loop, which is associated with “ink-bottle” type pores. These results suggest that there are copper species located on the surface of the PMOs causing partial pore blocking. This conclusion will be further confirmed by the EPR results.

Table 1. Chemical and physical structure parameters of the xCu-PMO samples under study

Sample	PMO	0.06Cu-PMO	0.10Cu-PMO	0.15Cu-PMO	0.20Cu-PMO	0.30Cu-PMO
Cu content	-	0.9%	1.8%	2.5%	3.5%	4.8%
Surface area (m^2g^{-1})	1014	845	778	706	646	572
De (nm)[a]	2.9	3.3	3.3	3.3	3.4	3.3
Dp (nm)[b]	2.9	3.5	3.5	3.6	3.8	3.8
Pore Volume (cm^3g^{-1})	0.83	0.75	0.68	0.60	0.59	0.49

a: Pore size at the entrance of the mesopores (calculated from the desorption branch)
b: Pore size of the cage (calculated from the adsorption branch)

HAADF-STEM images of Cu-PMO with a different amount of copper loading are presented in Figure 5. Since in the HAADF-STEM mode the intensity in the images is proportional to the squared atomic number (Z^2) of the elements under investigation and the thickness of the sample,[37] Cu-containing particles will appear brighter compared to the porous structure. For 0.06Cu-PMO (Figures 5a), it can thus be seen that the copper-containing nanospecies are well-dispersed in the material (the small bright features dispersed in the matrix). However, for 0.15Cu-PMO, larger bright particles can be observed in the HAADF-STEM image (Figure 5b), which correspond to the clustering of copper-containingmaterial. For 0.30Cu-PMO, a large amount of copper-containing clusters has been detected (Figure 5c). The representative elemental mapping (Si, O, Cu) of the 0.06Cu-PMO are given in the Supporting Information, Figure S4. Again it is clear that the Cu species are well dispersed in the sample, which is in agreement with the HAADF STEM images of this material. In order to determine the location of the copper-containing nanospecies, electron tomography needs to be performed, since conventional TEM images only correspond to 2D projections of 3D objects. Therefore a tilt series of 65 HAADF-STEM images was acquired over a tilt range of -64^o to $+64^o$. This series was used as an input for a 3D reconstruction which is visualized in Figure 6a and 6b. From slices through the 3D reconstruction, such as the one presented in Figure 6b, it can be found that the copper-rich nanospecies are well dispersed in the material, not only on the outer surface, but also in the channels of the material.

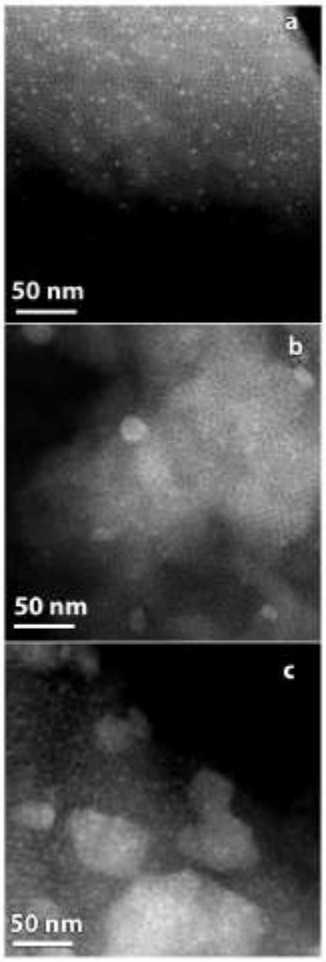

Figure 5. HAADF-STEM images of (a) 0.06Cu-PMO, (b) 0.15Cu- PMO and (c) 0.30Cu-PMO (bright dots are copper-containing nanospecies)

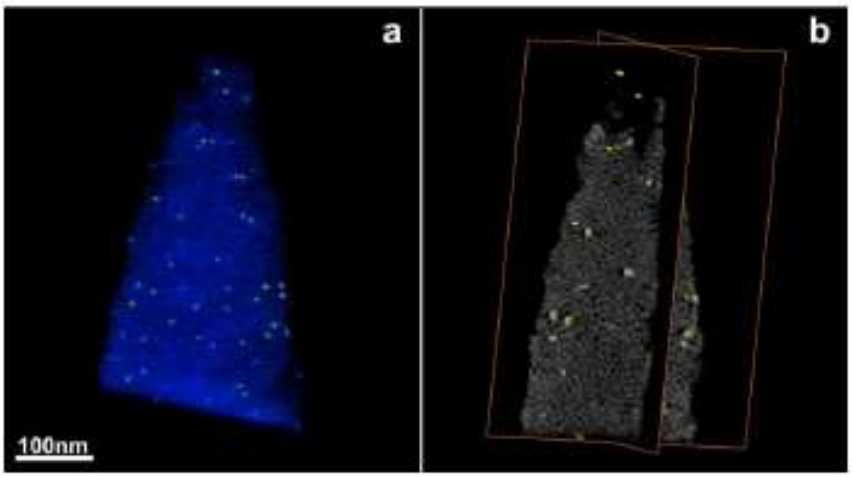

Figure 6. (a) 3D reconstructed volume of 0.06Cu-PMO, matrix rendered in blue, and the Cu nanoparticles in yellow. (b) Orthoslices through the reconstructed volume, the bright-contrast Cu nanoparticles are spread through the matrix.

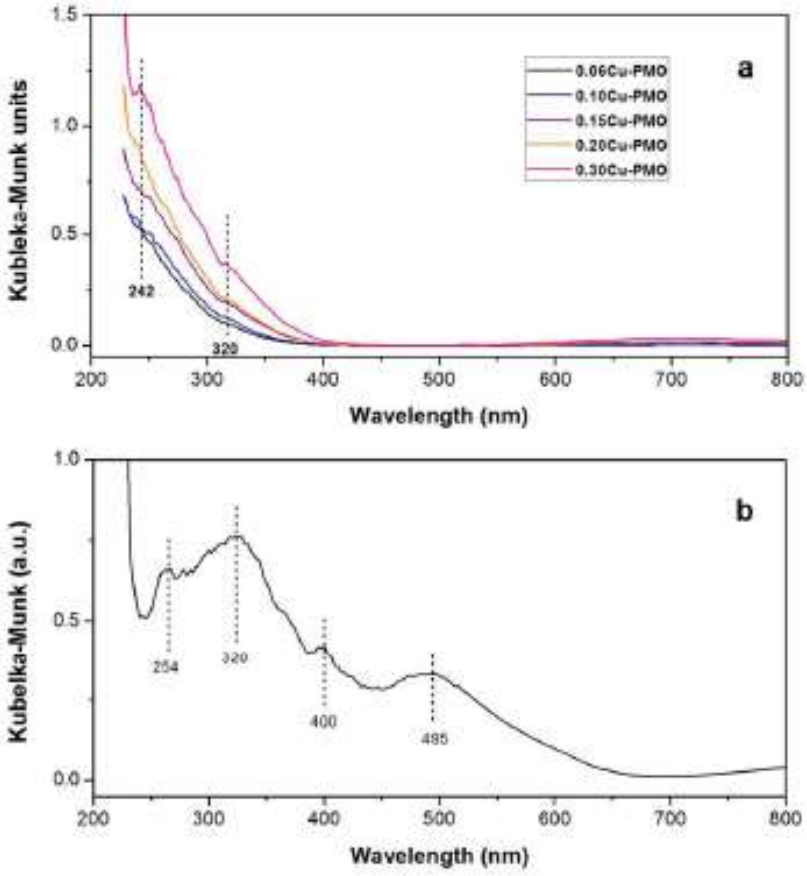

Figure 7. (a) UV-Vis-Dr spectra of (a) solvent-extracted xCu-PMO materials and (b) IM-Cu-PMO materials

UV-vis-Dr spectra of the Cu-PMOs are recorded in order to understand the nature of the coordination environment of the copper ions in the materials (Figure 7a). The intensity of the UV-Vis-Dr signal is growing with increasing copper amount. The UV-Vis-Dr spectrum of all studied Cu-PMOs can be fitted by two sub-bands. The first band centered at about 242 nm is related to the charge transfer between mononuclear Cu^{2+} ion and oxygen,[38-40] whereas the band centered round 320 nm can be assigned to a charge transfer between Cu^{2+} and oxygen in [Cu-O-Cu]n surface species.[23,41-43] Moreover, an additional broad band appears at about 680 nm for the Cu-PMOs with higher copper amount, which can be attributed to the d-d transition of Cu in an (pseudo-)octahedral environment in CuO.[38]

Figure 7b shows, as a comparison, the UV-Vis-Dr spectra of a copper-containing PMO material prepared by impregnation (IM-Cu- PMO, 2wt% copper). Besides the bands of the mononuclear Cu^{2+} ions, the oligonuclear [Cu-O-Cu]n and CuO species, two additional bands can be detected at about 400 and 495 nm. The band at about 400 nm is also related to the presence of CuO nanoclusters,[44] while the broad band at around 495 nm can be attributed to the d-d transition of Cu in an octahedral coordination.[23] These results indicate that mononuclear Cu^{2+} species are dominant in the Cu-PMO materials prepared via direct synthesis, while the copper species in IM-Cu-PMO have a large amount of oligonuclear [Cu-O-Cu]n and CuO species.

The above conclusion is supported by the EPR results. EPR provides a very powerful tool for obtaining information on the chemical environment and the coordination state of Cu^{2+} ions in different materials.[45-47] The EPR spectra also depend on the degree of the dispersion of the Cu^{2+} ions in the solid. Figure 8 shows the CW-EPR spectrum of IM-Cu-PMO (2 wt% copper) taken at room temperature and at 10K. The EPR spectrum of IM-Cu-PMO recorded at room temperature exhibits only a single feature, typical for strong spin-spin interactions between the Cu^{2+} ions, hence indicating that the copper ions are in close vicinity to each other (clustering). At low temperature, the spectrum changes and consists of two contributions: one broad signal which again is typical of dipolarly interacting Cu^{2+} ions, and a contribution of an isolated Cu(II) site, with g and 35Cu hyperfine parameters: gx=2.081 (±0.003), gy=2.084(±0.003), gz=2.407(±0.002), ^{Cu}Ax= ^{Cu}Ay =25 (±5) MHz, ^{Cu}Az=425 (±2) MHz. The latter contribution is very similar to the parameters known for [Cu(H2O)6]2+.48 This shows that part of the Cu^{2+} ions have mainly a water (or combined silanol and water) ligation. The observation of hexaquo copper also agrees with the observed leaching of copper when rinsing IM-Cu-PMO. Furthermore, the broad low-temperature and room-temperature EPR contributions confirm the presence of oligonuclear [Cu-O-Cu]n species and the formation of crystalline copper oxide in the IM-Cu- PMO material as derived from the powder XRD (Figure 3) and UVVis Dr measurements (Figure 7b). The spectrum in Figure 8a is also similar to that observed for nanostructured copper oxide in silicazirconia mixed oxides.[49]

The spectra of the IM-Cu-PMO material differ considerably from those observed for the xCu-PMO materials obtained through direct synthesis (Figure 9). Even at the highest copper loading, the spectra are still dominated by the characteristic spectrum of mononuclear Cu^{2+} sites. Increasing copper loading leads nevertheless to a gradual broadening of the EPR lines, which indicates an increase of the dipolar interactions (increase of local copper concentration

and clustering). This result is in agreement with the result of the UVVis- Dr spectra and TEM measurements, which have shown that, at higher copper- loading amount, oligonuclear [Cu-O-Cu]n species can be found in the Cu-PMO materials. For all xCu-PMO materials, the EPR spectra at 10 K and room temperature are typical of immobilized Cu^{2+} sites, indicating that the Cu^{2+} ions are strongly adsorbed onto the PMO wall or are part of the PMO framework wall.

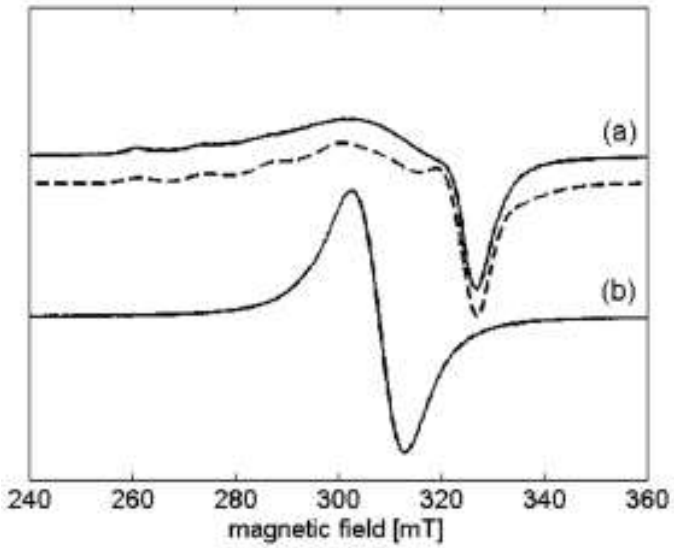

Figure 8. CW-EPR spectrum of IM-Cu-PMO recorded at (a) 10 K and (b) room temperature. The dashed line shows a simulation including two components: a broad line centered around g=2.14 and a contribution typical for a mononuclear Cu(II) complex (simulation parameters are given in the text). The spectra were taken with 10 mW microwave power.

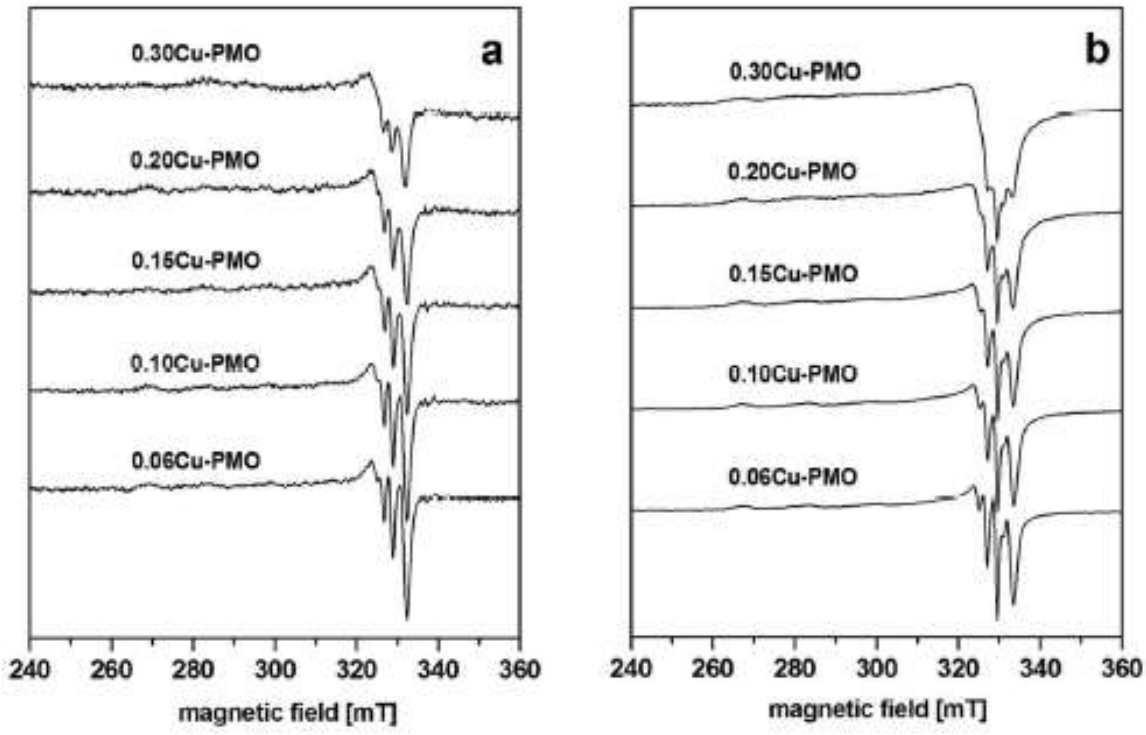

Figure 9. CW-EPR spectra of the solvent-extracted xCu-PMO sample recorded at room temperature (a) and 10 K (b). The spectra are normalized to allow easy comparison. The spectra are taken at 10 mW microwave power.

The EPR spectrum can be simulated assuming an isolated Cu(II) site, with the following g and ^{63}Cu hyperfine parameters: gx=2.054 (±0.002), gy=2.056 (±0.002), gz=2.315 (±0.003), ^{Cu}Ax= 55 (±3) MHz, ^{Cu}Ay =53 (±3) MHz, ^{Cu}Az=470 (±2) MHz. These values are typical of a Cu^{2+} in a square pyramidal or distorted octahedral environment with only oxygen atoms in the first coordination shell of the Cu2+ ion.[50] Furthermore, this site has a lower gz value and a higher ^{Cu}Az-value than the mononuclear contribution to the EPR spectrum of IMCu- PMO (Figure 8a). This indicates a more negative charge of the Cu^{2+} complex,[50] suggesting less water coordination and more coordination of deprotonated silanol groups (which indicates formation of Cu-O-Si linkages). The latter is supported by the 1H HYSCORE experiments performed on 0.06Cu-PMO (Figure 10). These experiments allow the identification of the hyperfine interaction between the unpaired electron and the nearby protons. The maximum width of the proton ridge is 4.4MHz, which is much smaller than the maximum proton coupling expected for equatorial water binding in a Cu^{2+} complex.[51] The observed ridge is, however, typical of axially coordinated water or -OH groups. This suggests that the Cu^{2+} ions

are accessible for solvent molecules and thus present at the silica surface. The absence of equatorially ligated water was also confirmed by the absence of the characteristic proton combination frequency in the two-pulse ESEEM spectra (not shown).

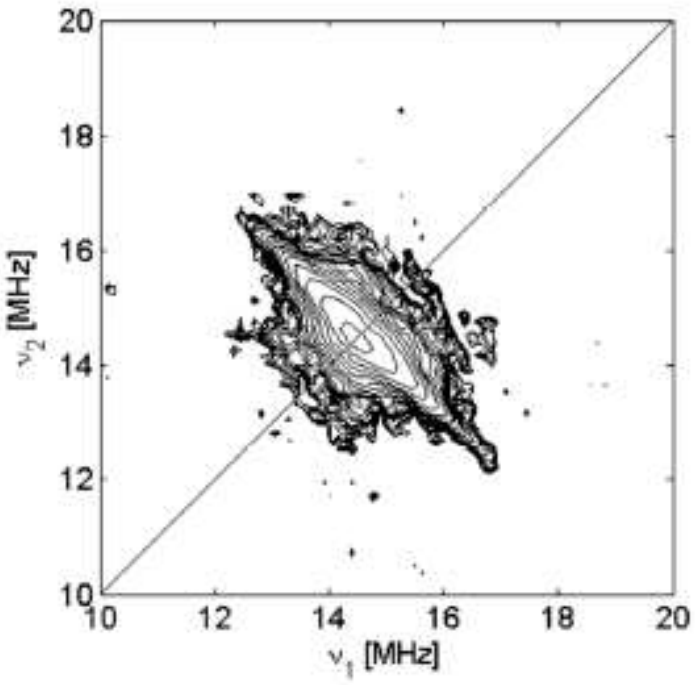

Figure 10. 1H HYSCORE spectrum of 0.06Cu-PMO recorded at 10 K at a magnetic field position agreeing with g=gx (339.8 mT). The spectrum is the sum of two τ values (104 and 154 ns).

EPR can also be used to follow the evolution of the copper incorporation during the PMO synthesis. Figure 11 shows the room temperature EPR spectra taken at different stages of the 0.06Cu- PMO synthesis. The top, red spectrum stems from the reaction mixture before addition of BTEE, but with all other components present. It shows the typical four-line isotropic spectrum that is found for a fast tumbling of Cu(II) complex. From this spectrum, the isotropic giso (=(gx+gy+gz)/3) value and the isotropic copper hyperfine value, $^{Cu}A_{iso}$ (=(^{Cu}Ax+ ^{Cu}Ay + ^{Cu}Az)/3), can be derived. For the initial Cu(II) complex (red spectrum in Figure 11), g_{iso} = 2.122 (±0.002) and $^{Cu}A_{iso}$ = 197 (±1) MHz. giso is considerably lower than the one observed after template removal in 0.06Cu-PMO (g_{iso} =2.142; value computed from g-tensor analysis in Figure 9). This decrease is typically observed when nitrogen atoms instead of oxygen atoms are bound to the copper.[50] This illustrates the initial ligation of the

Cu^{2+} ion with ammonia. When BTEE is added to the solution, we observe a change of the EPR spectrum in time. The lines broaden and new low-field signals appear (see arrows in Figure 11). These are typical indications of the decrease of motion of the Cu^{2+} ion/complex as the PMO is formed (incorporation of the copper ion). This reduction of the motion of the copper complex becomes clearly observable after the first hour of reaction. These results indicate that the immobilization of the Cu^{2+} ion/complex and the formation of the PMO material happen simultaneously. Since the formation of a Si-O-Si bond is much easier than the formation of a Si-O-Cu bond, it is difficult to incorporate Cu^{2+} ions into the framework of the PMO material. The copper ions tend to stay on the inner surface of the mesopores, being coordinated with the lattice oxygen, which explains the EPR observations for the final xCu-PMOs (Figures 9,10).

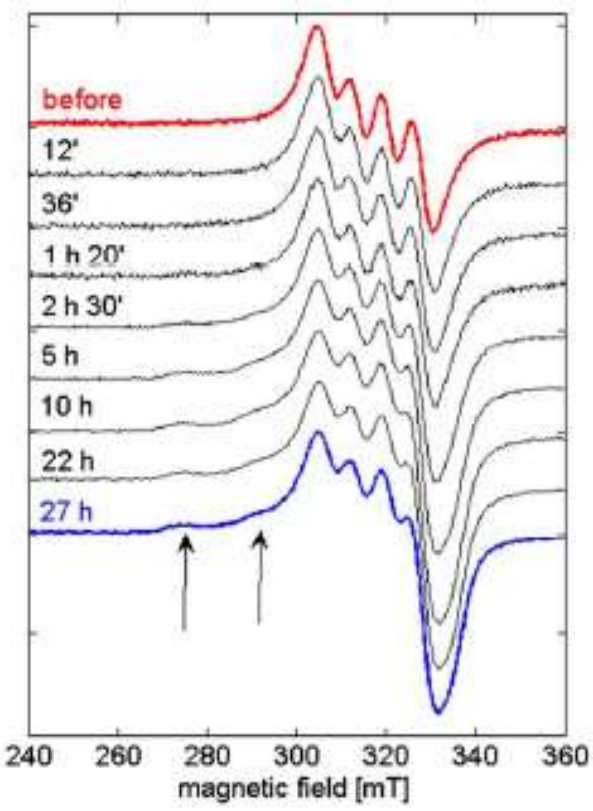

Figure 11. Evolution of the room temperature EPR spectra during the synthesis of 0.06Cu-PMO. The top, red spectrum shows the reaction mixture without BTEE, all other spectra depict the reaction mixture (with BTEE) after different times of stirring the solution.

Figure 12 shows the comparison between the EPR spectra of the synthesis mixture of 0.06Cu-PMO after 27h, the filtered-off material still including the template, and the final 0.06Cu-PMO material after template removal. We notice the following effects. While the spectra of the two former samples (Figure 12a, b) still show the presence of fully mobile Cu2+ ions, these are totally removed during the template removal (Figure 12c). This indicates that these mobile species are freely moving inside the template micelles, which confirms our earlier assumption on the penetration of the Cu(NH3)4 2+ complexes into the micelles. The relative amount of fast rotating Cu2+ complexes is larger in the synthesis mixture (Figure 12a) than after filtration of the powder in line with the concomitant detection of these species in the EPR spectra of the filtrate (not shown).

Secondly, we see a clear change in the EPR parameters of the immobilized Cu(II) sites (illustrated for instance by the shift of the low-field feature indicated by the arrow in Figure 12). Different effects contribute to these spectral changes. In the reaction mixture, the synthesized PMO particles are still present in suspension. These particles (and any Cu(II) complex immobilized in it) will still be able to freely move in the suspension, albeit much slower than the individual molecular copper complexes. Upon filtering, the powder is immobilized which causes a related change of the EPR spectrum. Furthermore, the EPR spectrum is also influenced by the type of the complexing ligands.[50] The large change observed between the immobilized Cu(II) contributions in spectra 12b and 12c is due to the removal of the template and ammonia as ligands for the copper ion. This change confirms the earlier conclusion that the copper ions are situated at the PMO surface and that they are accessible to molecules. Similar spectral changes were observed for Cu- and Al-containing MCM-41.52 While the EPR spectrum of Cu-AlMCM-41 after adsorption of NH3 was characterized by gz=2.245 and ^{Cu}Az=537 MHz (g_{iso} = 2.120), adsorption of methanol led to a strong spectral change (gz=2.377, ^{Cu}Az=448 MHz, giso=2.180).

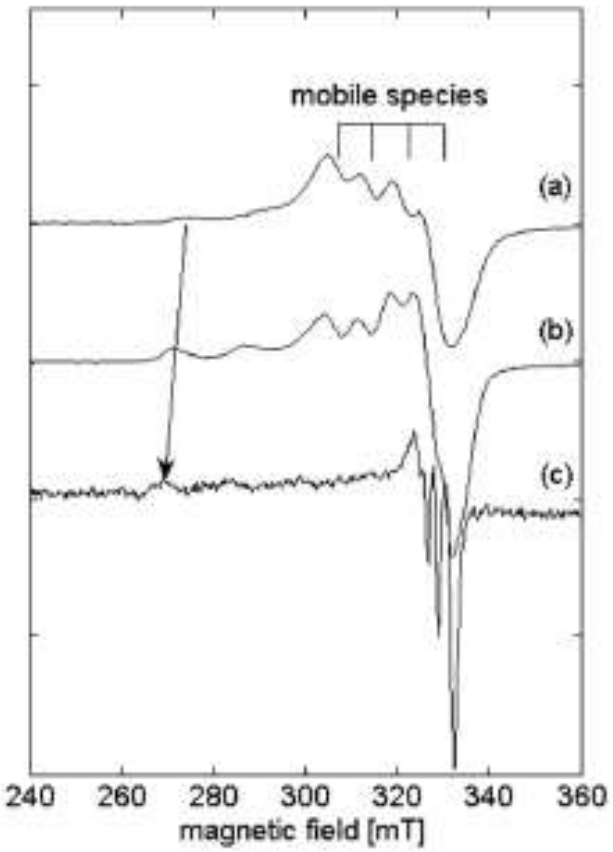

Figure 12. Room temperature CW EPR spectrum of the synthesis mixture of 0.06Cu-PMO after 27h (a), the filtered-off material still including the template (b), and the final 0.06Cu-PMO material after template removal (c). The four-line contribution of the immobilized species is indicated. The arrow shows the shift in the low-field feature.

Conclusion

In summary, a facile direct-synthesis method of copper-containing ethane-bridged PMO materials (xCu-PMO) has been described. The nature and distribution of the Cu^{2+} species in the materials were investigated in detail through a wide number of physicochemical characterization techniques, including XRD, UV-Vis-Dr, TEM, CWEPR and pulsed EPR spectroscopy. A comparison is made with a Cu-containing ethane-bridged PMO obtained by copper impregnation. The latter material is heterogeneous containing oligonuclear [Cu-O-Cu]n species and crystalline copper oxide. The material also contains hexaquo copper complexes that are probably responsible for the copper leaching. The xCu-PMO materials have, however, better defined structures. The physicochemical analysis shows that at lower copper loading, the Cu^{2+} species are well dispersed in the Cu-PMO materials, and mainly

exist as mononuclear Cu^{2+} species. At higher copper loading amount, Cu^{2+} clusters are also formed in the materials, but the distribution of the Cu^{2+} species is still much more homogeneous than in the Cucontaining PMO material prepared through the impregnation method. Furthermore, EPR revealed that the copper ions are situated on the inner surface of the mesopores of the materials and are accessible, which will be beneficial for future catalytic applications.

Acknowledgements

The Erasmus Mundus CONNEC program is acknowledged for PhD funding of F.Lin. Furthermore, the authors acknowledge support by the GOA-BOF project 'Optimization of the structure-activity relation in nanoporous materials', funded by the University of Antwerp. S.B. acknowledges the European Research Council for funding under the European Union's Seventh Framework ERC grant agreement n° 335078-COLOURATOM.

Notes and references

Electronic Supplementary Information (ESI) available: [1] TEM images of the copper-free PMO material, [2] The representative elemental mapping (Si, O, Cu) of the 0.06Cu-PMO. See DOI: 10.1039/b000000x/

[1] T. Asefa, M.J. MacLachlan, N. Coombs, G.A. Ozin, Nature, 1999, 402, 867-871.

[2] S. Inagaki, S. Guan, Y. Fukushima, T. Ohsuna, O. Terasaki, J. Am. Chem. Soc., 1999, 121, 9611-9614.

[3] T. Asefa, M.J. MacLachlan, H. Grondey, N. Coombs, G.A. Ozin, Angew. Chem. Int. Edit, 2000, 39, 1808-1811.

[4] F. Hoffmann, M. Cornelius, J. Morell, M. Froba, Angew. Chem. Int. Edit,2006, 45, 3216-3251.

[5] Q.H. Yang, J. Liu, L. Zhang, C. Li, J. Mater. Chem.,2009, 19, 1945- 1955.

[6] B.J. Hughes, J.B. Guilbaud, M. Allix, Y.Z. Khimyak, J. Mater. Chem., 2005, 15, 4728-4733.

[7] Q.H. Yang, Y. Li, L. Zhang, J. Yang, J. Liu, C. Li, J. Phys. Chem. B, 2004, 108, 7934-7937.

[8] M.P. Kapoor, A. Bhaumik, S. Inagaki, K. Kuraoka, T. Yazawa, J. Mater. Chem., 2002, 12, 3078-3083.

[9] A. Bhaumik, M.P. Kapoor, S. Inagaki, Chem. Commun., 2003, 4, 470- 471.

[10] J.A. Melero, J.M. Arsuaga, P.G. de Frutos, J. Iglesias, J. Sainz, S. Blazquez, Micropor. Mesopor. Mat., 2005, 86, 364-373.

[11] W. Guo, X.S. Zhao, Micropor. Mesopor. Mat., 2005, 85, 32-38.

[12] B.J. Hughes, J.-B. Guilbaud, M. Allix, Y.Z. Khimyak, J. Mater. Chem., 2005, 15, 4728.

[13] S. Shylesh, P.P. Samuel, A.P. Singh, Micropor. Mesopor. Mat., 2007, 100, 250-258.

[14] M.P. Kapoor, A. Bhaumik, S. Inagaki, K. Kuraoka, T. Yazawa, J. Mater. Chem., 2002, 12, 3078-3083.

[15] H. Chu, Y. Wan, D. Zhao, Catal. Today, 2009, 148, 19-27.

[16] J.A. Melero, J. Iglesias, J.M. Arsuaga, J. Sainz-Pardo, P. de Frutos, S. Blazquez, J. Mater. Chem., 2007, 17, 377.

[17] S. Shylesh, A.P. Singh, Micropor. Mesopor. Mat., 2006, 94, 127-138.

[18] S. Shylesh, C. Srilakshmi, A.P. Singh, B.G. Anderson, Micropor. Mesopor. Mat., 2007, 99, 334-344.

[19] C.M. Chanquia, K. Sapag, E. Rodriguez-Castellon, E.R. Herrero, G.A. Eimer, J. Phys. Chem. C, 2010, 114, 1481-1490.

[20] L. Wang, A. Kong, B. Chen, H. Ding, Y. Shan, M. He, J. Mol. Catal. A-Chem, 2005, 230, 143-150.

[21] B.Y. Chou, J.L. Tsai, S.F. Cheng, Micropor. Mesopor. Mat., 2001, 48, 309-317.

[22] G. Moretti, C. Dossi, A. Fusi, S. Recchia, R. Psaro, Appl. Catal. BEnviron, 1999, 20, 67-73.

[23] L. Chmielarz, P. Kuśtrowski, R. Dziembaj, P. Cool, E.F. Vansant, Appl. Catal. B-Environ, 2006, 62, 369-380.

[24] C.C. Liu, H.S. Teng, Appl. Catal. B-Environ, 2005, 58, 69-77.

[25] R.J.P. Corriu, A. Mehdi, C. Reye, C. Thieuleux, Chem. Commun., 2003, 13, 1564.

[26] X. Zheng, M. Wang, Z.Q. Sun, C. Chen, J.P. Ma, J. Xu, Catal. Commun., 2012, 29, 149-152.

[27] P. Schlossmacher, D. O. Klenov, B. Freitag, H. S. Von Harrach, Microsc. Today, 2010, 18, 14-20.

[28] W.J. Palenstijn, K.J. Batenburg, J. Sijbers, J. Struct. Biol., 2011, 176, 250-253.

[29] P. Höfer, A. Grupp, H. Nebenfuhr, M. Mehring, Chem. Phys. Lett., 1986, 132, 279-282.

[30] S. Stoll, A. Schweiger, J. Magn. Reson., 2006, 178, 42-55.

[31] C.L. Tsai, B. Chou, S. Cheng, J.F. Lee, Appl. Catal. A-Gen, 2001, 208, 279-289.

[32] K. Schumacher, P.I. Ravikovitch, A. Du Chesne, A.V. Neimark, K.K. Unger, Langmuir, 2000, 16, 4648-4654.

[33] X.B. Zhang, J. Li, B. You, G.P. Yong, H.W. Tong, S.M. Liu, Rsc Adv., 2012, 2, 9778-9780.

[34] Q.S. Huo, D.I. Margolese, G.D. Stucky, Chem. Mater., 1996, 8, 1147-1160.

[35] H. Song, R.M. Rioux, J.D. Hoefelmeyer, R. Komor, K. Niesz, M. Grass, P.D. Yang, G.A. Somorjai, J. Am. Chem. Soc., 2006, 128, 3027-3037.

[36] M. Trejda, A. Tuel, J. Kujawa, B. Kilos, M. Ziolek, Micropor. Mesopor. Mat., 2008, 110, 271-278.

[37] S. J. Pennycook, Ultramicroscopy, 1989, 30, 58-69.

[38] S. Velu, L. Wang, M. Okazaki, K. Suzuki, S. Tomura, Micropor. Mesopor. Mat., 2002, 54, 113-126.

[39] D. Rath, K.M. Parida, Ind. Eng. Chem. Res., 2011, 50, 2839-2849.

[40] F.M.T. Mendes, M. Schmal, Appl. Catal. A-Gen, 1997, 151, 393-408.

[41] S. Velu, K. Suzuki, M. Okazaki, M.P. Kapoor, T. Osaki, F. Ohashi, J. Catal., 2000, 194, 373-384.

[42] M. Iwamoto, H. Yahiro, N. Mizuno, W.X. Zhang, Y. Mine, H. Furukawa, S. Kagawa, J. Phys. Chem.-Us, 1992, 96, 9360-9366.

[43] M.R. Prasad, G. Kamalakar, S.J. Kulkarni, K.V. Raghavan, J. Mol. Catal. A-Chem, 2002, 180, 109-123.

[44] Y.L. Dong, X.Y. Niu, Y.J. Zhu, F.L. Yuan, H.G. Fu, Catal. Lett., 2011, 141, 242-250.

[45] M.F. Ottaviani, S. Bossmann, N.J. Turro, D.A. Tomalia, J. Am. Chem. Soc., 1994, 116, 661-671.

[46] M.A. Karakassides, A. Bourlinos, D. Petridis, L. Coche-Guerente, P. Labbe, J. Mater. Chem., 2000, 10, 403-408.

[47] C.M. Chanquia, E.L. Winkler, M.T. Causa, G.A. Eimer, J. Phys. Chem. C, 2012, 116, 5376-5382.

[48] L. Trouillet, T. Toupance, F. Villain, C. Louis, Phys. Chem. Chem. Phys., 2000, 2, 2005-2014.

[49] D.B. Dell'Amico, H. Bertagnolli, F. Calderazzo, M. D'Arienzo, S. Gross, L. Labella, M. Rancan, R. Scotti, B.M. Smarsly, R. Supplit, E. Tondello, E. Wendel, Chem-Eur. J., 2009, 15, 4931-4943.

[50] J. Peisach, W.E. Blumberg, Arch. Biochem. Biophys., 1974, 165, 691-708.

[51] P.M. Schosseler, B. Wehrli, A. Schweiger, Inorg. Chem., 1997, 36, 4490-4499.

[52] A. Pöppl, M. Hartmann, L. Kevan, J. Phys. Chem.-Us, 1995, 99, 17251-17258.